Online Estimation of Linearized IBR models using Ambient Noise and External Excitation

Mriganka Mukherjee, Santosh V. Singh, A. M. Kulkarni, Kaustav Dey, Aniruddha M. Gole

***Abstract*—Inverter-based resources (IBRs) are now an increasingly important component of modern power grids. However, as the penetration of IBRs increases, several real-life instances of instability or nuisance oscillations are being reported. High-fidelity small-signal models can greatly help to diagnose, anticipate, and mitigate these problems. This paper proposes a scheme for the online small-signal model estimation of IBRs using external excitation signals and/or ambient noise as probing signals. These excitation signals can be realized through small-amplitude wide-band set-point modulation of power electronic equipment such as IBRs, FACTS, or HVDC converters in the vicinity. The linearized models of IBRs so obtained can be combined with the impedance of the transmission network and other devices to predict the stability of the overall system. This paper describes the signal processing algorithms used in the scheme and discusses the practical implementation issues. Proof-of-concept Electro-Magnetic Transient (EMT) simulation studies are presented, and the effect of various parameters are analysed.**

***Keywords*—Inverter-based resources, admittance frequency response estimation, system identification, Spectral analysis, multi-coherence based identification.**

I. Introduction

Power electronic inverters are a crucial component for interfacing renewable energy systems, FACTS, and HVDC transmission systems with the AC grid. While they provide enhanced control flexibility, their widespread adoption has raised stability concerns due to the possibility of adverse interactions; several instances of undamped oscillations between IBRs and other power system components have been reported in the literature [1], [2]. These adverse interactions can be mitigated through controller parameter modifications and the use of supplementary damping controllers [3].

In most cases, the undamped oscillations arise due to small-signal instabilities. Linear time-invariant (LTI) models valid for small excursions around the equilibrium can be used to analyze such oscillations. Frequency domain LTI models can be extracted using simulations or online experiments by injecting small-amplitude wide-band signals probing signal(s) into the system and measuring the responses [4]. These IBR models are typically obtained in the form of frequency responses of Multi-Input Multi-Output (MIMO) transfer functions obtained in the D-Q domain. The overall system can be built in a modular fashion: the D-Q domain MIMO admittance of individual IBRs can be extracted and combined with the electrical network impedance to obtain the frequency response of the overall system. This can then be used to determine the stability of the system. Since the underlying system is non-linear, the IBR models are operating point-dependent. However, the network impedance transfer function is linear, and it can be obtained analytically in a straightforward manner.

The models required to accurately diagnose, anticipate, and mitigate stability problems need to have high fidelity. Therefore, even if analytical models are available, they need to be validated experimentally. *In situ* probing to estimate the parameters of passive power apparatus like transformers can be done offline, i.e., when the apparatus is out of service [5]. Online probing is more meaningful for IBRs as the aim is to extract a small-signal model around a quiescent operating condition, which is available if the IBR is energized and in service. Such estimation of models requires external probing signals. Probing signal injection has been used previously for online transformer testing [6] and low-frequency modal estimation in power systems [7]. It is also used in experimental model estimation of automatic voltage regulators [8].

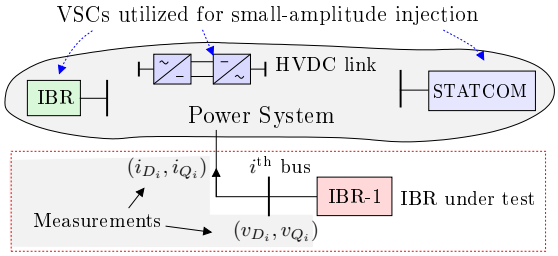

Fig. 1: Online model estimation facilitated by remote excitation.

This paper proposes the use of other Voltage Source Converters (VSC) based IBRs, HVDC or FACTS converters in the vicinity of the IBR under test to inject small-amplitude currents into the system. This is achieved by modulating the set point of their fast-acting current controllers with suitably designed signals. The model of the IBR under test is estimated using the measured signals at that IBR. The scheme is depicted in Fig. 1. Unlike the simulation-based frequency scanning [4], which is done in a controlled environment, online estimation is affected by ambient noise. Major sources of this noise are consumer-initiated load variations/switching and naturally occurring disturbances. While ambient noise contaminates the test signals, it could potentially be used to aid the estimation if its statistical properties are stationary during the tests.

This paper lays the signal processing groundwork for the estimation procedure and brings out the practical implementation issues. The cross-power spectral density (CPSD)-based algorithm is used, which is suitable under noisy ambient

Mriganka Mukherjee, Santosh V. Singh, and A. M. Kulkarni are with the Department of Electrical Engineering, Indian Institute of Technology Bombay, Mumbai-400076, India (e-mail: mriganka@iitb.ac.in, santoshvsingh68@gmail.com, anil@ee.iitb.ac.in).

Kaustav Dey and Aniruddha M. Gole are with the Department of Electrical and Computer Engineering, University of Manitoba, Canada (e-mail: kaustav.dey@umanitoba.ca (corresponding author), aniruddha.gole@umanitoba.ca).

Paper submitted to the International Conference on Power Systems Transients (IPST2025) in Guadalajara, Mexico, June 8-12, 2025.

conditions. A multi-coherence function is used to assess the reliability of the estimated model. Simulation case studies are presented to demonstrate how the estimation scheme works.

II. D-Q Models of the Network and IBRs

The aim of the online model estimation is to obtain the transfer function of an IBR at its terminals. The model is extracted in the D-Q domain, as the underlying system is time-invariant in this frame under balanced operating conditions [9]. The D-Q transformation in (1) transforms the a-b-c variables to the D-Q-o variables. The variable x can denote either voltage or current, and $\gamma = \omega_o t + \xi$, ξ being an arbitrary constant.

$$\begin{bmatrix} x_D \\ x_Q \\ x_o \end{bmatrix} = \sqrt{\tfrac{2}{3}} \begin{bmatrix} \cos(\gamma) & \cos(\gamma - \frac{2\pi}{3}) & \cos(\gamma - \frac{4\pi}{3}) \\ \sin(\gamma) & \sin(\gamma - \frac{2\pi}{3}) & \sin(\gamma - \frac{4\pi}{3}) \\ \frac{1}{\sqrt{2}} & \frac{1}{\sqrt{2}} & \frac{1}{\sqrt{2}} \end{bmatrix} \begin{bmatrix} x_a \\ x_b \\ x_c \end{bmatrix} \quad (1)$$

The frequency used in the D-Q transformation ω_o is taken to be the prevailing steady-state frequency so that the D-Q variables are constants in the steady state.

A. Network Model

The transmission network can be modeled as a balanced circuit with R-L-C elements for control interaction studies. It can be represented as a multi-port transfer function in the ($\alpha-\beta$) variables obtained by applying Clarke's transformation [10] to the corresponding a-b-c quantities.

$$\begin{bmatrix} \Delta V_{\alpha\beta_1} \\ \vdots \\ \Delta V_{\alpha\beta_n} \end{bmatrix} = \begin{bmatrix} Z_{\alpha\beta_{11}}(s) & \cdots & Z_{\alpha\beta_{1n}}(s) \\ \vdots & & \\ Z_{\alpha\beta_{n1}}(s) & \cdots & Z_{\alpha\beta_{nn}}(s) \end{bmatrix} \begin{bmatrix} \Delta I_{\alpha\beta_1} \\ \vdots \\ \Delta I_{\alpha\beta_n} \end{bmatrix} \quad (2)$$

The prefix 'Δ' denotes small deviations from the equilibrium. Each element of the impedance matrix given above ($Z_{\alpha\beta_{ij}}$) is a 2×2 sub-matrix relating a 2×1 voltage vector $V_{\alpha\beta_i}$ to a 2×1 current vector $I_{\alpha\beta_j}$, the other currents being zero.

$$\begin{bmatrix} \Delta V_{\alpha_i}(s) \\ \Delta V_{\beta_i}(s) \end{bmatrix} = \begin{bmatrix} Z_{ij}(s) & 0 \\ 0 & Z_{ij}(s) \end{bmatrix} \begin{bmatrix} \Delta I_{\alpha_i}(s) \\ \Delta I_{\beta_j}(s) \end{bmatrix} \quad (3)$$

where $\Delta V_{\alpha\beta_i} = [\Delta V_{\alpha_i}\ \Delta V_{\beta_i}]^T$ and $\Delta I_{\alpha\beta_j} = [\Delta I_{\alpha_j}\ \Delta I_{\beta_j}]^T$. If the impedance matrix in the D-Q variables is represented as follows,

$$\begin{bmatrix} \Delta V_{Di}(s) \\ \Delta V_{Qi}(s) \end{bmatrix} = \begin{bmatrix} Z_{DD_{ij}}(s) & Z_{DQ_{ij}}(s) \\ Z_{QD_{ij}}(s) & Z_{QQ_{ij}}(s) \end{bmatrix} \begin{bmatrix} \Delta I_{D_j}(s) \\ \Delta I_{Q_j}(s) \end{bmatrix} \quad (4)$$

then, from the relationship between the α-β and the D-Q variables, we obtain the following relationship [10],

$$\begin{aligned} Z_{DD_{ij}}(s) = Z_{QQ_{ij}}(s) &= \frac{Z_{ij}(s + j\omega_o) + Z_{ij}(s - j\omega_o)}{2} \\ Z_{DQ_{ij}}(s) = -Z_{QD_{ij}}(s) &= \frac{Z_{ij}(s + j\omega_o) - Z_{ij}(s - j\omega_o)}{2j} \end{aligned} \quad (5)$$

B. IBR model

Assuming balanced conditions and neglecting harmonics, the IBR model in the D-Q variables is time invariant [9] and can be treated as a linear system for small levels of signal excitation. This yields the small signal model of the IBR as given in (6). For a single-port IBR connected at bus i of the network as shown in Fig. 1,

$$\begin{bmatrix} -\Delta I_{Di}(s) \\ -\Delta I_{Qi}(s) \end{bmatrix} = \begin{bmatrix} Y_{DD_{ii}}(s) & Y_{DQ_{ii}}(s) \\ Y_{QD_{ii}}(s) & Y_{QQ_{ii}}(s) \end{bmatrix} \begin{bmatrix} \Delta V_{D_i}(s) \\ \Delta V_{Q_i}(s) \end{bmatrix} \quad (6)$$

where the current is *injected* into the network by the IBR.

C. Overall System Model

The network impedance model is linear and can be analytically derived; it depends only on the topology and network parameters and not on the power flows. The IBR models have to be extracted and stored for different operating conditions. An operating condition is characterized by the real and reactive power injection by the IBR, as well as the voltage and frequency at its terminals. The model of each IBR at the various system operating conditions is combined with the transmission network model (which can be analytically obtained) to obtain the model of the overall system as shown in Fig. 2. These combined system models can be used to determine the stability at these operating conditions. A lookup table consisting of damping and resonant frequencies at different operating conditions could be constructed for the operator. If an operating condition with poor damping is encountered, then the operator could steer the system to the closest safe operating point by carrying out set point changes in the IBR(s).

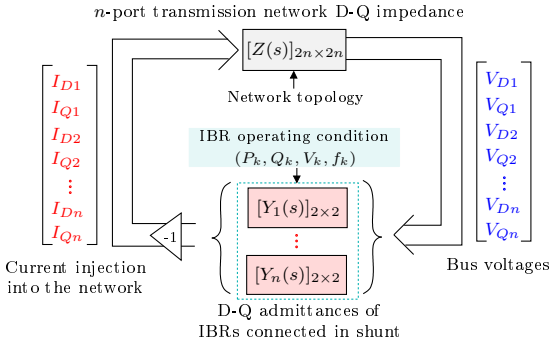

Fig. 2: Combining the models of IBRs and other system components.

Remarks

1) D-Q Reference Frame: For interaction studies involving multiple IBRs, the impedance and admittance matrices should be obtained using a *common* D-Q frame. This is because, in general, the angle ξ in the D-Q transformation (1) affects the individual terms of the admittance matrix in the D-Q variables. If a 2×2 admittance matrix in the D-Q frame Y_A is obtained using a D-Q transformation with $\xi = \xi_A$, and Y_B is obtained using $\xi = \xi_B$, then Y_A and Y_B are related by the following equation, where $\delta = \xi_2 - \xi_1$.

$$Y_B = \begin{bmatrix} \cos\delta & -\sin\delta \\ \sin\delta & \cos\delta \end{bmatrix} \times Y_A \times \begin{bmatrix} \cos\delta & \sin\delta \\ -\sin\delta & \cos\delta \end{bmatrix} \quad (7)$$

The matrices Y_A and Y_B are equal only if their diagonal terms are equal and the off-diagonal terms are equal in magnitude but of opposite sign. A similar condition holds true for the impedances.

For a passive electrical network, both the admittances and impedances satisfy these properties, as evident in (5). However, this is not true for IBRs, and synchronous generators [11].

Therefore, if the IBR admittances are to be combined with transfer functions of other IBRs and the transmission network for interaction studies, they should use a transformation derived from a *common clock* with equal values of ξ. This is possible to achieve using GPS-based timing signals, which can provide a theoretical accuracy of synchronization better

than 1 μs. This is adequate when the bandwidth of the model to be extracted is, say, from 0 to 100 Hz.

2) Stability Analysis: The IBR admittance matrix is conveniently obtained by the process of frequency scanning, as discussed in the following section. This yields the values of the matrix components at $s = j\,\Omega = j\,2\,\pi \times f$ for different values of f, which typically range from 0−100 Hz for controller interaction studies. This frequency range is sufficient because instabilities associated with interactions between IBRs and the network usually lie in the range of 0-100 Hz. The transfer function poles could be obtained via the process of "vector fitting" of the frequency response matrix to a rational transfer function matrix [12], from which the system's stability can be inferred. Alternatively, the frequency response could be used directly to determine stability using the Generalized Nyquist Criterion [13]. The inferences must be drawn carefully, as the model is estimated only for a finite range of frequencies.

III. Estimation of IBR Model

A. Simulation-based model estimation

If a black-box simulation model of an IBR is available that can be probed only at its terminals, then its small-signal frequency response can be obtained using time-domain simulation tools as indicated in Fig. 3. This technique is commonly known as frequency scanning [4], [14]. In this method, the signal injection is done directly at the IBR terminals by adding a controlled voltage source, as shown in the figure.

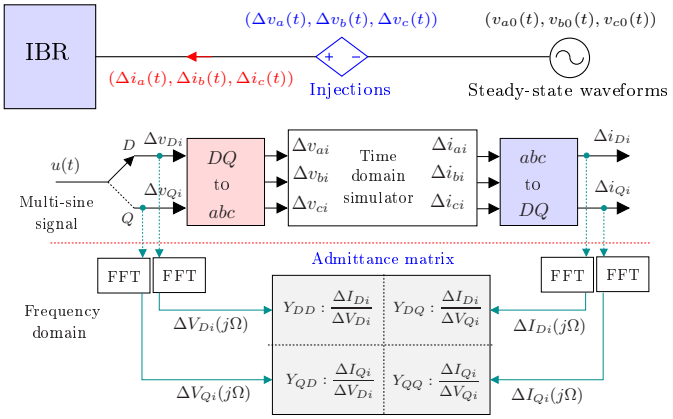

Fig. 3: Estimation of transfer functions using frequency scanning.

A multi-sine probing signal of the following form can be used for the frequency scanning.

$$u(t) = \sum_{l=N_1}^{N_2} a_l \sin(2\pi l f_d t + \phi_l) \tag{8}$$

Note that this signal has $N_2 - N_1 + 1$ frequency components (from $N_1 f_d$ to $N_2 f_d$) each spaced by f_d Hz. Therefore, the fundamental period of $u(t)$ is $T_d = (1/f_d)$ s. The maximum amplitude of $u(t)$ has to be limited to avoid large deviations from the equilibrium. The parameters a_l and ϕ_l may be chosen appropriately to reduce the maximum amplitude, thereby avoiding nonlinear IBR behavior [15]. The effect of this choice is illustrated in Fig. 4. Fig. 4 (b) is desirable due to its smaller envelope.

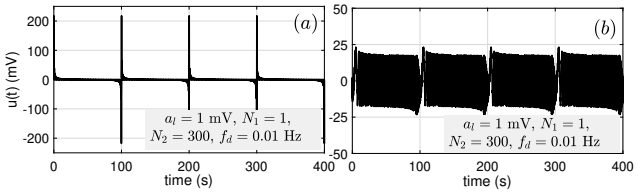

Fig. 4: Multi-sines: (a) $\phi_l = 0$, and (b) $\phi_l = -\frac{(l-N_1)(l-N_1+1)\pi}{N_2-N_1+1}$.

The steady-state response of the system to the low-amplitude multi-sine injection is periodic with a period T_d. The Fast Fourier Transform (FFT) algorithm [16] is generally used to determine the frequency components of the measured currents and voltages after the natural transients have died down. The FFTs of the periodic injected and measured signals are then obtained over a data window spanning one fundamental period or integral multiples of the period of the multi-sine.

Models extracted using simulation-based frequency scanning have proven to be quite useful and accurate [17], but validating these models through physical testing is desirable. This can be achieved using online methods as described below.

B. Online Model estimation using Probing Signals

Online small-signal model estimation can be done through tests and measurements on an actual IBR (not the simulation model) that is in service and is energized. While the wide-band test signals could be directly injected at the terminals of the IBR as done in the simulation-based method, it would require coupling the signal generation equipment to the high-voltage system via injection transformers.

A more convenient and inexpensive way of doing this testing is to use other VSC-based devices in the vicinity for injecting the signals (see Fig. 1), obviating the need for special equipment. Set point modulation of the inner current controllers of these devices with multi-sine signals can help to achieve this. The inner current controllers are usually present in all VSC-based grid-connected power electronic systems and are fast-acting. Therefore, they can facilitate wide-band current injection into the system. The candidate signal injection points in a typical grid-forming IBR are shown in Fig. 5.

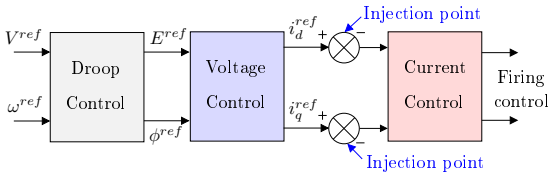

Fig. 5: Candidate injection points for multi-sine signals in an IBR.

Remarks:

1) Minimum Independent Injections: The estimation of the four components of the 2×2 admittance matrix of a single-port IBR would require at least two independent (*non-simultaneous and distinct*) injections. For example, in the simulation-based model estimation of Fig. 3, the D-Q currents are obtained for the $\Delta v_D(t)$ injection first and then for the $\Delta v_Q(t)$ injection.

In the case of excitation implemented by modulating the real or reactive current of remote IBRs, at least two independent injections are required that give linearly independent Δv_D

and Δv_Q spectra at the terminals of the IBR under test. The measurements of the D-Q currents and voltages (four measurements) at the terminals for the two injection tests can then yield the desired admittance matrix components.

For example, one multi-sine signal could be injected at the set-point of the real current controller of a remote IBR, while at a later time (i.e., independent of the first injection) another signal could be injected at the reactive current controller of that IBR. The use of more than the minimum (two injections) number of experiments can help to reduce the effects of noise, which can be done by involving multiple remote IBRs. The model can then be extracted from the over-determined system of equations using methods like total least squares.

2) Active Power Injection: The small-amplitude modulation of the set points of the real current (current in phase with voltage) will cause corresponding variations in the instantaneous real power exchange between the VSC injection device and the system. However, since the multi-sine signals have a zero average, the net energy required for this is essentially zero. Nevertheless, these real power variations will cause variations in the DC link capacitor voltage of the VSC. Hence, the amplitude of real current modulation should be restricted. Reactive power modulation is less restrictive, as it does not result in power modulation on the DC side of the VSC.

C. Online Ambient Noise based estimation

Ambient sources of excitation like naturally-occurring disturbances and consumer-initiated load-switching noise (which is continually present) are generally considered a nuisance in model estimation using probing signals. However, it may be possible to utilize noise for model estimation when statistical methods are employed. Note that the aggregated load variations, which is a major source of noise in power systems, can be treated as band-limited white noise [18]. Ambient noise-based estimation, if feasible, could obviate the need for probing signal injection at the other IBRs. Ambient noise and naturally occurring disturbances have been used for estimating the frequency and damping of low-frequency swing modes [7] and for transformer frequency response estimation [19], [20].

Intuitively, the scheme seems viable if the noise or transient disturbances have spectral components of sufficient magnitude in the frequency range of interest. Long data records are generally required for accurate noise-based estimation. Even with this approach, a minimum of two uncorrelated noise sources that give linearly independent Δv_D and Δv_Q spectra are required. Fortunately, since a power system has a large number of loads at different buses acting independently, this condition is usually satisfied.

IV. Signal Processing Steps for Model Estimation

A. FFT-based estimation

For each independent injection scenario k carried out under a given operating condition, the following equation is satisfied for each frequency component ($s = j\Omega$ rad/s) of the voltages and currents obtained using FFT.

$$[\Delta I_{DQ_i}(j\Omega)]_k = -\begin{bmatrix} \Delta V_{DQ_i}(j\Omega)_k & [0] \\ [0] & \Delta V_{DQ_i}(j\Omega)_k \end{bmatrix} \begin{bmatrix} Y_{DD}(j\Omega) \\ Y_{DQ}(j\Omega) \\ Y_{QD}(j\Omega) \\ Y_{QQ}(j\Omega) \end{bmatrix} \quad (9)$$

where, $\Delta V_{DQ}(j\Omega)_k = \begin{bmatrix} \Delta V_D(j\Omega) & \Delta V_Q(j\Omega) \end{bmatrix}_k$ and $[\Delta I_{DQ}(j\Omega)]_k = \begin{bmatrix} \Delta I_D(j\Omega) & \Delta I_Q(j\Omega) \end{bmatrix}_k^T$. Note that the subscript 'i' denoting the bus at which the IBR under test is connected is omitted to avoid notational clutter.

Each injection should be carried out for a duration of time which spans several windows of duration T_d. A few initial windows are discarded to allow the natural transients to decay. The measurements will be contaminated by ambient noise, which will affect the estimation. Therefore, the measurements are averaged over several non-overlapping time windows of period T_d *before* computing the FFT. Ideally, this will improve the signal-to-noise ratio (SNR) by a factor equal to the number of windows that are averaged [21].

Two independent injections ($k = 1, 2$) carried out sequentially will yield four equations to solve for the unknowns Y_{DD}, Y_{DQ}, Y_{QD} and Y_{QQ}, as given in (9). As discussed in Section III-B, this is the minimum number required to obtain the four admittance components. Additional (independent) injection tests are likely to yield better estimates in the presence of noise in both the current and voltage measurements. The over-determined set of equations resulting from these additional tests, which are of the form $Ax = b$, can be solved using the *total least squares* formula. The TLS solution is obtained as shown in (10).

$$x_{tls} = -\frac{R(1:n, n+1)}{R(n+1, n+1)} \quad (10)$$

R is a $(n+1) \times (n+1)$ matrix obtained from the singular value decomposition, $[A\ b] = P\ \Sigma\ R^H$, where $[A\ b]$ is an $n \times (n+1)$ matrix obtained by appending the column vector b to the matrix A. P is a $n \times n$ matrix and Σ is a diagonal matrix containing the singular values. The superscript 'H' denotes the conjugate transpose operation.

B. Cross Power Spectral Density based estimation

As an alternative to the FFT-based approach, one may use a Cross Power Spectral Density (CPSD) based approach to estimate the frequency response. The advantage of the CPSD-based scheme over the "plain" FFT-based scheme of Section IV-A is that it can potentially leverage the ambient noise to aid the estimation.

The CPSD S_{xy} between two signals $\Delta x(t)$ and $\Delta y(t)$ is defined as follows.

$$S_{xy}(j\Omega) = \text{FFT}(\texttt{xcorr}(\texttt{Δx(t)}, \texttt{Δy(t)})) \quad (11)$$

where $\texttt{xcorr}(\texttt{Δx(t)}, \texttt{Δy(t)})$ denotes the cross-correlation between $\Delta x(t)$ and $\Delta y(t)$ [22]. The record duration is chosen to be long enough so that $S_{xy}(j\Omega)$ is relatively constant in the frequency range of interest. For injection tests using multi-sine periodic signals of fundamental frequency f_d, multiples of its period T_d can be used for the computation of $S_{xy}(j\Omega)$, after the natural transients have died down.

The CPSD of the voltages and currents obtained from the k^{th} data record are related as follows.

$$\begin{bmatrix} S_{i_D - v_D}(j\Omega) \\ S_{iD - vQ}(j\Omega) \\ S_{i_Q - v_D}(j\Omega) \\ S_{iQ - vQ}(j\Omega) \end{bmatrix}_k = \begin{bmatrix} S_{v_{DQ}}(j\Omega)_k & [0] \\ [0] & S_{v_{DQ}}(j\Omega)_k \end{bmatrix} \begin{bmatrix} Y_{DD}(j\Omega) \\ Y_{DQ}(j\Omega) \\ Y_{QD}(j\Omega) \\ Y_{QQ}(j\Omega) \end{bmatrix} \quad (12)$$

where $S_{v_{DQ}}(j\Omega)_k = \begin{bmatrix} S_{v_D-v_D}(j\Omega) & S_{v_Q-v_D}(j\Omega) \\ S_{v_D-v_Q}(j\Omega) & S_{v_Q-v_Q}(j\Omega) \end{bmatrix}_k$ and $[0]$ denotes a 2×2 matrix of zeros.

The admittances can be uniquely obtained if $S_{v_{DQ}}(j\Omega)_k$ is of rank 2 at each frequency. It is easy to verify that this is not true for a data record obtained from a single multi-sine injection test with no ambient noise. Therefore, two or more records ($k = 1, 2, ..$) corresponding to independent multi-sine injection tests are used to form a system of equations that will yield the four admittance components.

Even if no multi-sine injection tests are performed using the external VSC devices, two or more uncorrelated external sources of noise, e.g., caused by load switching at different buses, can, in principle, be used for the CPSD-based estimation (see Section III-C). However, this requires measurement record lengths over which statistical properties like cross-correlation do not vary significantly. In practical implementations, the data record is often divided into windows. The CPSD estimates obtained for each of these windows are then averaged to get a smoother estimate [23].

C. Multi-Coherence Function

The IBR model estimation schemes presented in the previous sections rely on excitation sources external to the IBR, with no internal changes (like set point changes) occurring in the IBR under test. However, even if there are no internal changes in the IBR, measurement noise and non-linearities in the IBR response will cause errors in the estimation. The coherence function [24] is generally used to determine the extent to which the measurement noise and non-linearities are responsible for what is observed in the measurements. Consider the estimation of the two-input, two-output system IBR model given in (6), taking Δv_D and Δv_Q as the inputs, and Δi_D and i_Q as the outputs. The coherence function can be evaluated for the outputs, one at a time, as shown in (13).

$$\gamma^2{}_{X-i_D}(j\Omega) = \frac{S^H_{X-i_D}(j\Omega)\, S^{-1}_{X-X}(j\Omega)\, S_{X-i_D}(j\Omega)}{S_{i_D-i_D}(j\Omega)}$$

$$\gamma^2{}_{X-i_Q}(j\Omega) = \frac{S^H_{X-i_Q}(j\Omega)\, S^{-1}_{X-X}(j\Omega)\, S_{X-i_Q}(j\Omega)}{S_{i_Q-i_Q}(j\Omega)} \tag{13}$$

where, $S_{X-X}(j\Omega) = \begin{bmatrix} S_{v_D-v_D}(j\Omega) & S_{v_D-v_Q}(j\Omega) \\ S_{v_Q-v_D}(j\Omega) & S_{v_Q-v_Q}(j\Omega) \end{bmatrix}$;

$$S_{X-i_D}(j\Omega) = \begin{bmatrix} S_{v_D-i_D}(j\Omega) \\ S_{v_Q-i_D}(j\Omega) \end{bmatrix};\ S_{X-i_Q}(j\Omega) = \begin{bmatrix} S_{v_D-i_Q}(j\Omega) \\ S_{v_Q-i_Q}(j\Omega) \end{bmatrix}.$$

The multi-coherence function for each output lies between 0 and 1. It equals 1 at all frequencies if there is no measurement noise and nonlinearity. If it is significantly below 1, then it indicates that measurement noise and/or non-linearities are present and are at least partly responsible for what is observed in the measurements; in such a case, the estimates are unreliable. The estimations then have to be discarded and this has to be repeated with re-calibrated injections.

D. Practical Considerations

The IBR model estimation scheme requires consideration of several practical issues, which are summarized as follows.

1) Injection Sources: A prerequisite for this scheme is the accessibility of test signal injection points in the controllers. Considering the importance of model validation, it is imperative to include the provision of such injection points as a part of the specifications/regulations for IBR controllers. In this context, it is important to note that the signal injection by modulating the current controller set point of an IBR can also yield the necessary information for the design of a Supplementary Damping Controller for that IBR [3].

As discussed earlier, the signal injection should preferably be done where it is unlikely to be significantly attenuated by the controller, e.g. the summing point of the high-bandwidth inner current controller. However, attenuation at certain frequencies cannot be completely ruled out as it depends on the specific controller and the network characteristics. Inadequate excitation at some frequencies may result in poorer estimates at those frequencies. Therefore, the online estimation should preferably be based on several diverse excitation sources, including the natural ambient noise due to load variations.

The proposed approach is scalable for large power systems, as frequency domain models are generated using the measurements of each IBR over a range of operating conditions. The stability of the overall system can be obtained offline by combining the individual IBR models with the analytically obtained network model. A few IBRs are needed to provide the necessary excitation. In a large network, the excitation sources should preferably be near the IBR under test to ensure adequate signal amplitude at those IBR locations for measurement.

2) Measurement Instrument and Signal Conditioning: Measuring equipment with sufficient bandwidth and precision is necessary to capture the low amplitude variations. To capture the steady-state perturbations with higher precision, the voltage and current measurements should be passed through an analog notch filter to eliminate the large fundamental frequency component. The measured signals should also be low-pass filtered to avoid aliasing. Washout or de-trending filters are necessary to remove the variations below the bandwidth of interest due to slow generation and load changes.

3) Amplitude of Signal Injection: The IBR model is assumed to be linear for small levels of signal excitation and time-invariant in the D-Q variables. The linearity assumption may be violated if the variations at the terminal of the IBR under test (due to the excitation at other locations) are large, or if the IBR is operating close to the thresholds of non-linear blocks (like limiters) in its controller. This will cause distortions in the frequency response, which may result in inaccurate inferences. However, such situations can be identified using the multi-coherence function (Section IV-C), and the estimation can be repeated with a reduced injection signal.

The injection magnitude should be such that it results in responses whose amplitudes are about the same or higher than the ambient noise to be measurable using practical instrumentation. At the same time, the excitation should not affect normal operation or cause equipment limits to be hit during the estimation process. In practice, the voltage and current measurements will also be contaminated by ambient noise, which could affect the estimation. This can be reduced

by the signal processing techniques discussed in Section IV. To prevent excessively large magnitudes of the excitation input, the multi-sine signal given in (8) can be further optimized by utilizing the additional degree of freedom in the amplitudes of the individual frequency components. Offline simulation studies done prior to the online estimation can help determine appropriate levels of excitation and the accuracy of the estimation in the presence of noise.

4) Model Estimation Algorithm: In an ideal noise-free environment, the CPSD-based estimation would give results identical to the FFT-based method. However, in the presence of noise, the "conventional" FFT and CPSD algorithms differ in one key aspect. In a real-world system, the FFT would be inaccurate due to noise pollution, which can be alleviated to some extent by averaging the signal over several cycles (the effectiveness of this depends on the noise properties).

In contrast to the noise being an unwanted irritant that creates error, it is actually welcome in the CPSD approach which uses it to yield the system model. In this method, the frequency components of the cross-correlations of the measured signals are used to compute the frequency responses. The CPSD indirectly extracts the stationary properties of the noisy input and output measurements (through the FFT of the *correlation* of the signals). Therefore, CPSD can potentially exploit the noise if the noise is stationary.

5) Validation of Results: The estimated model of each IBR can be validated by comparing the inferences with the behaviour of the actual system. For example, the resonant frequency and damping obtained from the system model can be compared with the corresponding system measurements. If the reference model of the IBR is provided by the original equipment manufacturer (OEM) or can be obtained through testing, this can be used as a benchmark for the estimated model. If the OEM has provided a "Digital Twin" [25], i.e., a black-boxed EMT model, then the validation could also be done by comparing with this model. If such reference models are not available, the coherency measures in Section IV-C can be used as an index to determine whether the estimated models are affected by internal noise or non-linearities.

V. Simulation Case Studies

The IEEE 9-bus system with 100% renewable energy penetration, developed on the Electro-Magnetic Transients (EMT) simulation program PSCAD [26] by the National Renewable Energy Laboratory (NREL) [27] is utilized for this study. The system operates at 230 kV and supports a total load of 315 MW and 115 MVAr distributed among three IBRs. Fig. 6 depicts the schematic of the three-IBR system. Two of these IBRs - IBR-1 and IBR-2 function as Grid Forming (GFM) inverters, while IBR-3 operates as a Grid Following (GFL) inverter. The GFM inverters are equipped with active and reactive power droop controllers, which determine the set points of a voltage controller, which then determine the set points of the inner current control loop as shown in Fig. 5. The GFL inverter supplies real and reactive power based on externally specified set points.

We seek to estimate the model of IBR 3. The set points of the current controllers, both IBR 1 and IBR 2, are selected

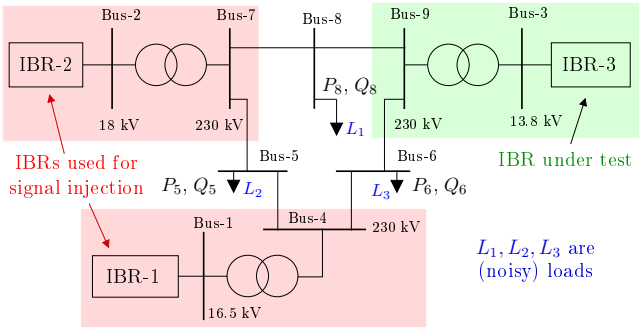

Fig. 6: Example system for the case studies.

as the candidate injection points for multi-sine signals. The maximum amplitude of the multi-sine envelope is taken to be 1% of the current rating of the IBR. The loads at buses 5, 6, and 8 (denoted by L_1, L_2 and L_3) are modelled as constant impedance loads with ambient noise injection. The standard deviation of the noise is about 1% of the quiescent value of the base load currents. Each injection test is carried out for 250 s. The measurements for the first 50 s have been excluded to allow for the natural transients to decay.

To assess the accuracy of the estimation with noise included, the frequency response obtained using the FFT and CPSD methods are compared with the reference (true) frequency response which is obtained using the approach shown in Fig. 3. It may not be possible to make such an idealized measurement in the field. Under such circumstances, the coherence function is useful to detect measurement contamination and non-linearity.

Various injection scenarios are considered as given in Table I. To get an idea of the deviations induced by the tests, the waveforms at IBR 3 terminals are shown in Fig. 7, for the test '1C'.

TABLE I: Cases considered.

Description/Multi-sine injection points(s)	FFT	CPSD
No Noise; IBR-1 $i_{d_{ref}}$ and $i_{q_{ref}}$	Case 1A	Case 2A
No Noise; IBR-1 $i_{d_{ref}}$ and $i_{q_{ref}}$, IBR-2 $i_{d_{ref}}$	Case 1B	Case 2B
Ambient Noise + IBR-1 $i_{d_{ref}}$	Case 1C	Case 2C
Ambient Noise + IBR-1 $i_{d_{ref}}$ and $i_{q_{ref}}$	Case 1D	Case 2D
Ambient Noise + IBR-1 $i_{d_{ref}}$ and $i_{q_{ref}}$, IBR-2 $i_{d_{ref}}$	Case IE	Case 2E
Ambient Noise; No Injection.	-	Case 2F

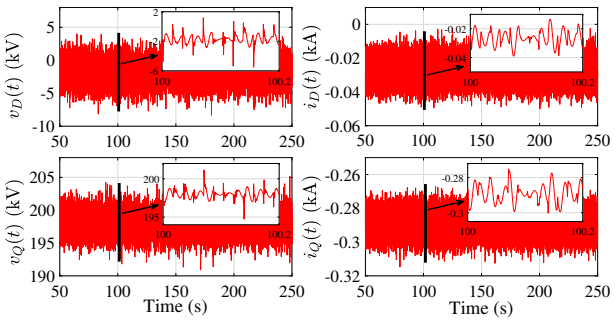

Fig. 7: Terminal quantities of the IBR under test (Case 1C).

A. Observations

1) The results for the FFT-based estimation are shown in Fig. 8. While the FFT-based method provides more accurate

estimates in controlled, low-noise environments, its performance degrades in the presence of ambient noise. With only one multi-sine injection (Case 1C) in the presence of noise, the FFT based method is unable to estimate the model correctly as expected.

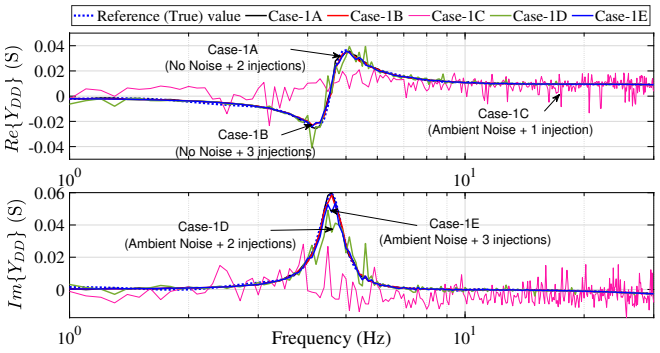

Fig. 8: Estimates using the FFT method of Section IV-A. Time-domain measurements over 20 non-overlapping windows of 10 s each are averaged before performing the FFT.

The results for CPSD-based estimation are shown in Fig. 9. In contrast to the FFT-based method, the CPSD-based method exhibits greater robustness under noisy conditions, including the only-noise case (2F). However, in this case (Case 2F), while the resonant frequency is correctly captured, the resonant peak is significantly lower than the true value.

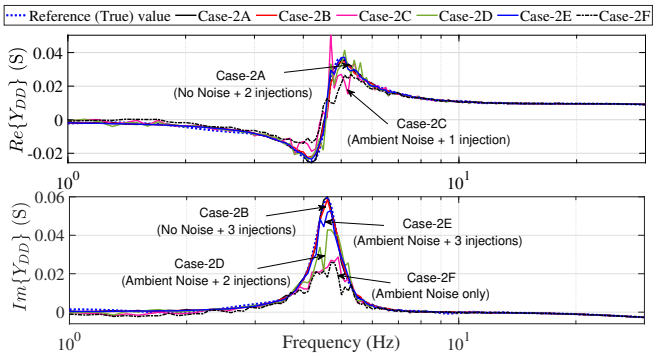

Fig. 9: Results using the CPSD method of Section IV-B. CPSDs over 20 non-overlapping windows of 10 s each are averaged.

2) The estimation accuracy for both methods is quantified using the Normalized Root Mean Square Error (NRMSE). The error is computed over the frequency range of 1 Hz to 10 Hz in which the resonant frequency lies. The NRMSE is estimated using a 0.1 Hz resolution for *each* admittance component is computed as follows.

$$\text{NRMSE (in \%)} = \frac{\sqrt{\frac{1}{N_f}\sum\left(\left|\hat{Y}(j\Omega)\right| - |Y(j\Omega)|\right)^2}}{\max\left(|Y(j\Omega)|\right)} \times 100 \qquad (14)$$

where $\hat{Y}(j\Omega)$ is the estimated admittance, $Y(j\Omega)$ is the reference admittance (obtained from frequency scan without noise), and the summation is over the frequency range of interest. The NRMSE values are shown in Table II. Note that T_r, N_w, and T_w denote the data record length, the number of data windows, and the length of each window, respectively.

TABLE II: NRMSE comparison for FFT and CPSD methods.

Case	T_r (s)	N_w	T_w (s)	Overlap	NRMSE (%) Y_{DD}	Y_{DQ}	Y_{QD}	Y_{QQ}
1D (FFT)	10	1	10	no	1.38	1.33	1.34	3.51
	100	10	10	no	1.31	1.12	1.45	1.27
	200	20	10	no	0.93	0.80	0.88	0.81
2D (CPSD)	200	5	40	no	0.38	0.37	0.35	0.44
	200	10	20	no	0.37	0.34	0.33	0.34
	200	20	10	no	0.38	0.33	0.32	0.34
	200	13	20	25%	0.37	0.31	0.32	0.32
	200	19	20	50%	0.36	0.27	0.30	0.27

For the cases with two injections and noise, the CPSD gives a more accurate estimate (Case 2D) compared to the FFT based estimate (Case 1D). Averaging the CPSD over a larger number of windows N_w seems to marginally improve the performance, although using overlapping windows does not seem to appreciably improve the results. In contrast, averaging of the signals in the time domain in the FFT method generally improves performance.

3) The multi-coherence functions (Section IV-C) are shown in Fig. 10 for two cases where ambient noise is also present. It is seen that the coherency values are generally good (above 0.75), except at frequencies lower than 1 Hz.

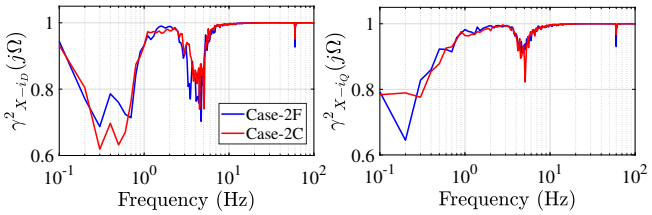

Fig. 10: Multi-Coherence functions for the cases 2C and 2F.

B. Effect of variation of excitation and ambient noise

To verify the effect of the magnitude of the excitation input and the ambient noise, the system is simulated with different levels of excitation input and ambient noise. In the first study, the ambient noise generated by load switching is kept constant at 1% (base case scenario). The amplitude of the excitation input is increased and decreased (by a factor of 2) from its value in the base case (1% of current rating). In the second study, the excitation level is kept constant while the noise level is increased and decreased by a factor of 2. The estimated frequency response of the Y_{DD} term using the FFT (Case 1D) and CPSD (Case 2D) approaches for the first study are shown in Fig. 11 and Fig. 12 respectively. The NRMSE values for both the studies are given in Table III. The frequency responses indicate that the error decreases with larger excitation, and vice versa. The reduced error for larger excitation indicates that non-linear behaviour is not significant for these excitation levels. The NRMSE values indicate that the SNR has a more significant impact on the FFT method than the CPSD method.

VI. Conclusions

This paper presents a framework for online model estimation of an IBR using excitation signals generated by other voltage-source converters in the vicinity of the IBR under test. Ambient noise caused by consumer load variations such as load switching can also potentially be used for this purpose. The paper describes two signal processing algorithms, one using FFT of the waveforms and the other using cross-power

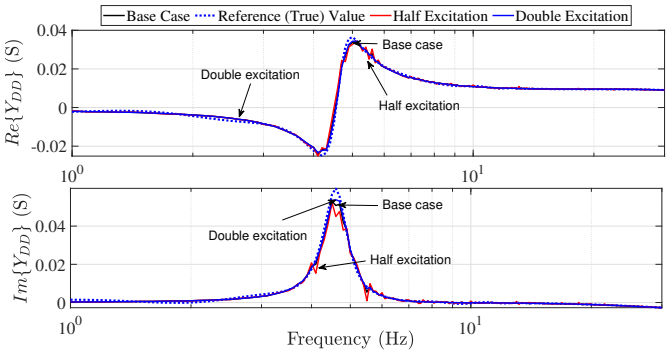

Fig. 11: FFT-based estimates for different excitation levels.

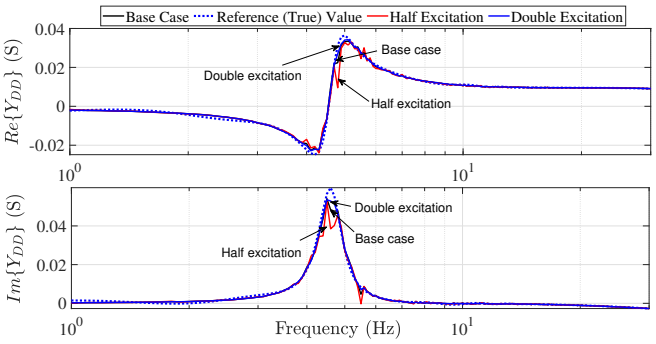

Fig. 12: CPSD-based estimates for different excitation levels.

TABLE III: NRMSE for FFT (1D) and CPSD (2D) methods.

	T_r	N_w	T_w	Method	NRMSE (%) Y_{DD}	Y_{DQ}	Y_{QD}	Y_{QQ}
Variation of excitation input								
1% noise, 0.5% excitation	200	10	20	**2D (CPSD)**	0.62	0.53	0.54	0.57
				1D (FFT)	1.01	1.04	1.10	1.05
1% noise, 1% excitation	200	10	20	**2D (CPSD)**	0.38	0.35	0.33	0.34
				1D (FFT)	0.93	0.80	0.88	0.81
1% noise, 2% excitation	200	10	20	**2D (CPSD)**	0.22	0.15	0.18	0.18
				1D (FFT)	0.21	0.14	0.18	0.17
Variation of noise level								
0.5% noise, 1% excitation	200	10	20	**2D (CPSD)**	0.2	0.16	0.18	0.17
				1D (FFT)	0.22	0.14	0.18	0.17
1% noise, 1% excitation	200	10	20	**2D (CPSD)**	0.38	0.35	0.33	0.34
				1D (FFT)	0.93	0.80	0.88	0.81
2% noise, 1% excitation	200	10	20	**2D (CPSD)**	1.57	1.39	1.49	1.64
				1D (FFT)	2.48	2.05	2.49	2.35

spectral density-based estimation. The latter approach (CPSD) is more recommended for field implementation as it works better in the presence of ambient noise. Simulation case studies demonstrate the scheme, with multi-sine injection tests and random load variations.

The results indicate that both the FFT and CPSD based methods can yield a good model estimate. The CPSD algorithm can leverage the ambient noise to obtain the estimate even without multi-sine injection signals, but the estimates are more accurate with the injection signals. In general, the accuracy of the methods is improved by averaging over several windows of the measurements. The simulation studies indicate that these methods hold promise and can be taken up for experimental validation.

REFERENCES

[1] S. H. Huang, J. Schmall, J. Conto, J. Adams *et al.*, "Voltage control challenges on weak grids with high penetration of wind generation: ERCOT experience," in *2012 IEEE Power and Energy Society General Meeting*, 2012, pp. 1–7.

[2] Y. Cheng, L. Fan, J. Rose, S. H. Huang *et al.*, "Real-world subsynchronous oscillation events in power grids with high penetrations of inverter-based resources," *IEEE Transactions on Power Systems*, vol. 38, no. 1, pp. 316–330, 2022.

[3] S. Ramachandra, K. Dey, A. Kulkarni, and A. M. Gole, "Frequency scanning based design of supplementary damping controllers for inverter-based resources," in *2024 IEEE Power & Energy Society General Meeting (PESGM)*. IEEE, 2024, pp. 1–5.

[4] X. Jiang and A. Gole, "A frequency scanning method for the identification of harmonic instabilities in HVDC systems," *IEEE Transactions on Power Delivery*, vol. 10, no. 4, pp. 1875–1881, 1995.

[5] K. Feser, et.al., "The transfer function method for detection of winding displacements on power transformers after transport, short circuit or 30 years of service," *CIGRE*, vol. 12, pp. 33–04, 2000.

[6] M. Bagheri, M. S. Naderi, and T. Blackburn, "Advanced transformer winding deformation diagnosis: moving from off-line to on-line," *IEEE Transactions on Dielectrics and Electrical Insulation*, vol. 19, no. 6, pp. 1860–1870, 2012.

[7] D. Trudnowski, D. Kosterev, and J. Wold, "Open-loop PDCI probing tests for the Western North American power system," in *2014 IEEE PES General Meeting — Conference & Exposition*, 2014, pp. 1–5.

[8] K. Bollinger and R. Gilchrist, "Voltage Regulator Models Using Automated Frequency Response Equipment," *IEEE Transactions on Power Apparatus and Systems*, vol. PAS-101, no. 8, pp. 2899–2905, 1982.

[9] C. Schauder and H. Mehta, "Vector analysis and control of advanced static VAR compensators," in *IEE Proceedings C-Generation, Transmission and Distribution*, vol. 140. IET, 1993, pp. 299–306.

[10] K. R. Padiyar, *Analysis of subsynchronous resonance in power systems*, 3rd ed. Springer Science & Business Media, 2012.

[11] K. Dey and A. M. Kulkarni, "Analysis of the Passivity Characteristics of Synchronous Generators and Converter-Interfaced Systems for Grid Interaction Studies," *International Journal of Electrical Power & Energy Systems*, vol. 129, p. 106818, 2021.

[12] B. Gustavsen and A. Semlyen, "Rational approximation of frequency domain responses by vector fitting," *IEEE Transactions on power delivery*, vol. 14, no. 3, pp. 1052–1061, 1999.

[13] A. G. MacFarlane and I. Postlethwaite, "The generalized Nyquist stability criterion and multivariable root loci," *International Journal of Control*, vol. 25, no. 1, pp. 81–127, 1977.

[14] A. M. Kulkarni, M. K. Das, and A. M. Gole, "Frequency scanning analysis of STATCOM-network interactions," in *2016 IEEE 6th International Conference on Power Systems (ICPS)*. IEEE, 2016, pp. 1–6.

[15] R. Pintelon and J. Schoukens, *System identification: a frequency domain approach*. John Wiley & Sons, 2012.

[16] A. V. Oppenheim and R. W. Schafer, *Digital Signal Processing*, 1st ed. Eaglewood Cliffs, NJ, 1975.

[17] K. Dey, M. K. Das, and A. Kulkarni, "Comparison of dynamic phasor, discrete-time and frequency scanning based SSR models of a TCSC," *Electric Power Systems Research*, vol. 196, p. 107237, 2021.

[18] G. Ledwich, T. Parveen, and P. O'Shea, "Measurement based Load Model Identification," in *Proceedings of the Symposium on Electrical Energy Evolution in China and Australia*, 2008.

[19] L. T. Coffeen, "System and method for on-line impulse frequency response analysis," Apr. 15 2003, US Patent 6,549,017.

[20] S. V. Singh, A. Kulkarni, and H. Bahirat, "Extraction of open-loop frequency response of power apparatus using transient data from multiple naturally occurring disturbances," *Electric Power Systems Research*, vol. 196, p. 107205, 2021.

[21] J. W. Pierre, N. Zhou, F. K. Tuffner, J. F. Hauer, D. J. Trudnowski, and W. A. Mittelstadt, "Probing Signal Design for Power System Identification," *IEEE Transactions on Power Systems*, vol. 25, no. 2, pp. 835–843, 2010.

[22] L. Ljung, *System identification*, 2nd ed. Springer, 1998.

[23] P. Welch, "The use of fast Fourier transform for the estimation of power spectra: A method based on time averaging over short, modified periodograms," *IEEE Transactions on Audio and Electroacoustics*, vol. 15, no. 2, pp. 70–73, 1967.

[24] J. S. Bendat and A. G. Piersol, *Random data: analysis and measurement procedures*, 4th ed. John Wiley & Sons, 2011.

[25] M. Zhou, J. Yan, and D. Feng, "Digital twin framework and its application to power grid online analysis," *CSEE Journal of Power and Energy Systems*, vol. 5, no. 3, pp. 391–398, 2019.

[26] 2010, Manitoba HVDC Research Centre, PSCAD/EMTDC Users guide, Winnipeg, Canada.

[27] R. W. Kenyon, A. Sajadi, A. Hoke, and B.-M. Hodge, "Open-source PSCAD grid-following and grid-forming inverters and a benchmark for zero-inertia power system simulations," in *2021 IEEE Kansas Power and Energy Conference (KPEC)*. IEEE, 2021, pp. 1–6.